第36卷第1期
2017年2月

红外与毫米波学报
J. Infrared Millim. Waves

Vol. 36, No. 1
February, 2017

文章编号: 1001 - 9014(2017)01 - 0024 - 06

DOI:10.11972/j.issn.1001 - 9014.2017.01.006

Design of TE_{01} -HE_{11} mode converter with TE_{11} as intermediary mode

FU Chen-Yang[1], LIAO Yong-Bo[1*], HE Yu-Zhen[2], YU Xin-Hua[3], NIU Xin-Jian[2]

(1. School of Energy Science and Engineering, University of Electronic Science and Technology of China, Chengdu 611731, China;
2. School of Physical Electronics, University of Electronic Science and Technology of China, Chengdu 610054, China;
3. School of Information and Communication, Guilin University of Electronic Technology, Guilin 541004, China)

Abstract: Based on the curved circular waveguide coupling theory and regular circular waveguide junction mode matching method, the TE_{01}-HE_{11} Mode Converter model was designed using the optimization parameter of the waveguide mode conversion structure obtained from relevant numerical calculation program, and was successfully simulated and verified by the CST software. The system is mainly composed of three parts: a TE_{01}-TE_{01} mode transition, two circular waveguide mode converters for TE_{01}-TE_{11} and TE_{11}-HE_{11}. The calculations showed that the conversion efficiency of the TE_{01}-HE_{11} mode converter system is over 99% within the bandwidth of 5% relative to 24.13 GHz. The results of simulations and test are consistent with that of calculation.

Key words: TE_{01}-TE_{01} mode transition, TE_{01}-TE_{11} mode conversion, TE_{11}-HE_{11} mode conversion, coupled wave theory, mode matching method

PACS: 52.35.Mw, 41.20.Jb, 41.20.-q, 07.57.-c

一种使用 TE_{11} 为过渡模的 TE_{01} -HE_{11} 模式变换器设计

付晨阳[1], 廖永波[1*], 何宇臻[2], 于新华[3], 牛新建[2]

(1. 电子科技大学能源科学与工程学院,四川 成都 611731;
2. 电子科技大学物理电子学院,四川 成都 610054;
3. 桂林电子科技大学信息与通信学院,广西 桂林 541004)

摘要:基于弯曲圆波导耦合理论和规则圆波导突变结构模式匹配法,利用 MATLAB 软件编写的相关数值计算程序得到波导模式转换结构的优化参量,最终使用 CST 软件对模型进行了仿真和验证. 该系统主要由三部分组成:一个 TE_{01}-TE_{01} 的过渡器,TE_{01}-TE_{11} 和 TE_{11}-HE_{11} 的圆波导模式转换器. 计算结果表明,该 TE_{01}-HE_{11} 模式转换系统在 24.13 GHz 的频率有 5% 的带宽、转换效率超过了 99%. 计算结果、仿真结果和实物冷测结果是一致的.

关 键 词:TE_{01}-TE_{01} 过渡器;TE_{01}-TE_{11} 模式转换器;TE_{11}-HE_{11} 模式转换器;耦合波理论;模式匹配法

中图分类号:TN811; TN814; TN128 **文献标识码**:A

Introduction

Gyrotron is a high-power microwave source, and it has a broad application prospect in aerospace, energy and other field.

In the 1980s, the high power mode converters were developed to convert the TE_{01} mode to the HE_{11} mode. Mode converters are necessary in some high-power microwave application since the output modes of gyrotrons are not the ideal transmission mode. Two kinds of conversion sequences are commonly adopted[1]:

1. TE_{0n} (gyrotron)-TE_{01} (Low loss transmission)-TE_{11}-HE_{11} (Antenna),

2. TE_{0n} (gyrotron)-TE_{01} (Low loss transmission)-TM_{11}-HE_{11} (Antenna).

This paper adopted the first conversion sequence,

Received date: 2016-05-06, **revised date**: 2016-08-31 **收稿日期**:2016-05-06, **修回日期**:2016-08-31

Foundation items: Supported by The National Natural Science Foundation of China (61571078, 61561013)

Biography: FU Chen-Yang (1993-), male, Nanyang, master. Research area involves high-power microwave (HPM) technology. E-mail: fuchy1103@qq.com

* **Corresponding author**: E-mail: lyb@uestc.edu.cn

that is, TE_{11} mode is the intermediary mode. In literature[2], an asymmetric mode converter TE_{01}-TE_{11} using Electric Field Integral Equation (EFIE) method has been designed and optimized. The optimized converter has a frequency band of 2.6% and its efficiency is higher than 95%. In literature[3], a TE_{01}-HE_{11} mode conversion system has been built to test launching HE_{11} microwave power into the plasma chamber. The conversion efficiency from TE_{01}-TE_{11} mode is 97%. This paper will present the research and design of a TE_{01}-HE_{11} mode converter system. Its conversion efficiency is over 99% and it has a broad bandwidth.

1 Theoretical analysis

1.1 Curved circular waveguide coupling theory

Based on the Maxwell's theory and the orthogonal function expansion theory, the corresponding coupled wave equations and the general expressions of coupling coefficient can be obtained[4-5]. The basic equation of the circular waveguide with axis bending can be written as[6]:

$$\frac{\mathrm{d}A^{+}_{m'n'}}{\mathrm{d}z} = -j\gamma_{m'n'}A^{+}_{m'n'} - j\sum_{mn}\left[C^{+}_{(m'n')(mn)}A^{+}_{mn} + C^{-}_{(m'n')(mn)}A^{-}_{mn}\right], \quad (1)$$

$$\frac{\mathrm{d}A^{-}_{m'n'}}{\mathrm{d}z} = j\gamma_{m'n'}A^{-}_{m'n'} + j\sum_{mn}\left[C^{+}_{(m'n')(mn)}A^{-}_{mn} + C^{-}_{(m'n')(mn)}A^{+}_{mn}\right], \quad (2)$$

where, $A^{+}_{m'n'}$ and $A^{-}_{m'n'}$ represent the amplitudes of the forward and backward waves of the $m'n'^{\mathrm{th}}$ mode, respectively. $C^{+}_{(m'n')(mn)}$ stands for the coupling coefficient between two modes (mn^{th} and mn modes) which have the same propagation direction, $C^{-}_{(m'n')(mn)}$ stands for the coupling coefficient between two modes (mn^{th} and $m'n'^{\mathrm{th}}$ modes) which have the opposite propagation directions. The expressions of coupling coefficient for circular waveguide $C^{\pm}_{(m'n')(mn)}$ are shown below[5]:

1) TE_{mn}-$TE_{m'n'}$ ($m' = m+1$)

$$C^{\pm}_{(m'n')(mn)} = \frac{(-1)^{m'n'}}{2(X'^{2}_{mn}-n^{2})^{1/2}[X'^{2}_{m'n'}-(n-1)^{2}]^{1/2}(X'^{2}_{m'n'}-X'^{2}_{mn})^{2}} \times \{(1\pm R_{mn}R_{m'n'})[2X'^{2}_{mn}X'^{2}_{m'n'}-m(m+1)(X'^{2}_{m'n'}+X'^{2}_{mn})] - \frac{X'^{2}_{mn}X'^{2}_{m'n'}}{(ka)^{2}}[X'^{2}_{m'n'}+X'^{2}_{mn}-2m(m+1)]\} \times \frac{ka}{R(R_{mn}R_{m'n'})^{1/2}} \quad (m>0)$$

$$C^{\pm}_{(m'n')(mn)} = \frac{X'_{mn}X'^{2}_{m'n'}(R_{mn}\pm R_{m'n'})^{2}}{2(R_{mn}\pm R_{m'n'})^{1/2}[X'^{2}_{m'n'}-(n+1)^{2}]^{1/2}(X'^{2}_{m'n'}-X'^{2}_{mn})^{2}} \times \frac{ka}{R}(-1)^{m+m'+1} \quad (m=0), \quad (3)$$

2) TE_{mn}-$TM_{m'n'}$ ($m' = m+1$)

$$C^{\pm}_{(m'n')(mn)} = \frac{-m(R_{mn}R_{m'n'})ka(-1)^{n+n'+1}}{2(R_{mn}\pm R_{m'n'})^{1/2}(X'^{2}_{mn}-m^{2}]^{1/2}(X^{2}_{m'n'}-X'^{2}_{mn})} \quad (m>0)$$

$$\begin{cases} n\neq n' & C^{\pm}_{(m'n')(mn)} = 0 \\ n=n' & C^{\pm}_{(m'n')(mn)} = \dfrac{(1\pm1)}{2\sqrt{2}X_{m'n'}}\times\dfrac{ka}{R} \end{cases} \quad (m=0), \quad (4)$$

where $R_{mn} = \dfrac{\beta_{mn}}{k}$. a is the waveguide radius, k is the free space wavenumber, and R is the curvature radius of the waveguide axis. X_{mn} is the nth zero of $J_m(X)$ (for TM modes) and X'_{mn} is the nth zero of $J'_m(X)$ (for TE modes).

The equation $\gamma_{m'n'} = \alpha_{m'n'} + j\beta_{m'n'}$ indicates the propagation constant of the $m'n'^{\mathrm{th}}$ mode, with $\beta_{m'n'}$ the wave number, $\alpha_{m'n'}$ the attenuation constant for circular waveguides, which determines the ohmic attenuation of waveguide. Those coupling coefficients above have been provided in the literature[7].

The expressions of attenuation constant for circular waveguides $\alpha_{m'n'}$ are shown below:

TM mode

$$\alpha_{m'n'} = \frac{1}{\alpha}\frac{R_s}{\eta_0}\frac{1}{\sqrt{1-\left(\dfrac{X_{m'n'}}{2\pi a}\lambda_0\right)^{2}}}, \quad (5)$$

TE mode

$$\alpha_{m'n'} = \frac{1}{\alpha}\frac{R_s}{\eta_0}\frac{1}{\sqrt{1-\left(\dfrac{X'_{m'n'}}{2\pi a}\lambda_0\right)^{2}}}\left[\left(\frac{X'_{m'n'}}{2\pi a}\lambda_0\right)^{2} + \frac{\left(\dfrac{m}{X'_{m'n'}}\right)^{2}}{1-\left(\dfrac{m}{X'_{m'n'}}\right)^{2}}\right], \quad (6)$$

where $X_{m'n'}$ is the n'^{th} zero of $J_{m'}(X)$ (for TM modes) and $X'_{m'n'}$ is the n'^{th} zero of $J'_{m'}(X)$ (for TE modes). a is the radius of waveguide. $\eta_0 = 376.7\Omega$, and it represents the impedance of free space wave. λ_0 is the wavelength of free space waves. R_s is the resistivity of the material of the waveguide. If length of mode converter is L, the boundary conditions of the converter would be:

$$A^{+}_{mn}\big|_{z=0} = [(1,0),(0,0),L(0,0)]^{\mathrm{T}}, \quad (7)$$

$$A^{-}_{mn}\big|_{z=L} = [(0,0),(0,0),L(0,0)]^{\mathrm{T}}, \quad (8)$$

A^{+}_{mn} is axis bending forward wave amplitude. A^{-}_{mn} is axis bending backward wave amplitude. Eq. 1, Eq. 2, Eq. 7 and Eq. 8 are constituted of boundary value problem of the coupling wave differential equations[8].

2 Mode Conversion System

2.1 Simulation and design of TE_{01} taper

The transition structure was designed based on the iterative synthesis. The transition profiles are shown in Fig. 1, and their starting radius and ending radius are 16.27 mm and 10.12 mm, respectively.

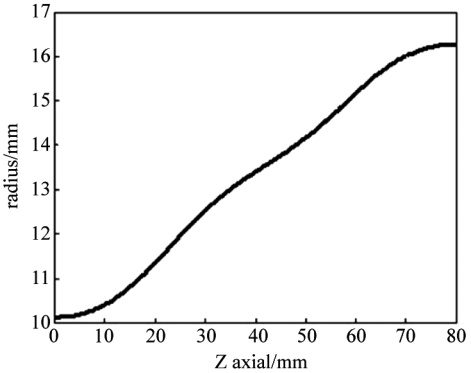

Fig. 1　Profile by optimizing calculation
图 1　优化后的过渡器轮廓

The TE_{01} power distribution along the transition axis is shown in Fig. 2. The frequency distribution diagram is shown in Fig. 3. The electric field distribution of the output port of the transition and longitudinal electric field distribution on the 2-D cut plane of the transition by the Microwave Studio CST software are shown in Fig. 4 and Fig. 5, respectively. The transmission efficiency is 99.89% at the frequency of 24.13 GHz. These results are in well agreement with those calculations.

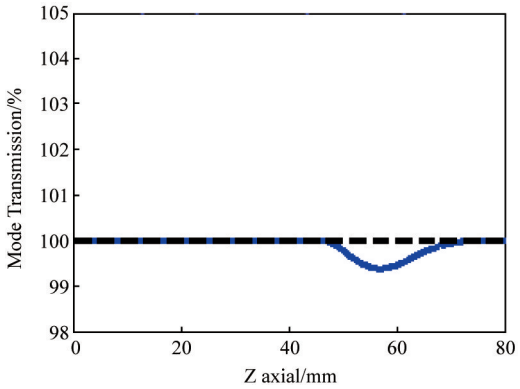

Fig. 2 Axis power distribution of TE_{01} mode
图2 TE_{01}模的轴向功率分布图

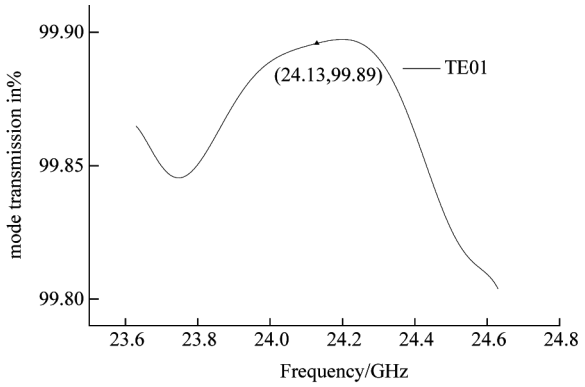

Fig. 3 Power distribution with the change of calculation frequency
图3 随频率变换的功率分布图

2.2 Simulation and design of TE_{01}-TE_{11} converter

Highly efficient conversion from TE_{01}-TE_{11} mode can be realized by the method of axis serpentine perturbation of a circular waveguide. The axial curve of the converter we designed is shown in Fig. 6. The converter has a radius of 10.12 mm and a length of 152.57 mm; it operates at the frequency of 24.13 GHz. Furthermore, the input and output port of the converter is aligned on the same axis.

To reduce the amplitude of other modes, we adopted the continuous phase matching techniques. Therefore, the whole converter length L should be

$$L = N\lambda_W \quad , \quad (9)$$

Where N is the number of perturbation period; $\lambda_W = (1+\delta)\cdot\lambda_B$ and it is different from the beat wavelength;

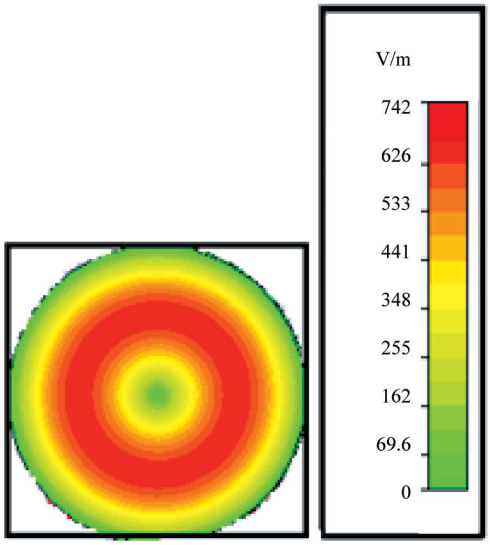

Fig. 4 Electric field distribution of the output port of the transition of the TE_{01} taper
图4 TE_{01}过渡器输出端口的电场分布图

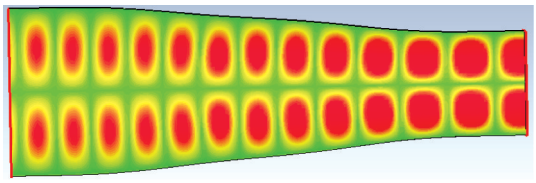

Fig. 5 Field distribution on the 2-D longitudinal output port of the transition cut plane of the TE_{01} taper
图5 二维切面纵向的TE_{01}过渡器输出端口电场分布图

$\lambda_B = \dfrac{2\pi}{|\beta_{TE_{01}} - \beta_{TE_{11}}|}$, it is the beat wavelength of TE_{01} mode and TE_{11} mode and δ is perturbation factor.

Some optimized factors such as high efficiency, coaxial and broad bandwidth were analyzed in the calculation to make the input and output port of the converter align on the same axis. The ohmic loss in the waveguide wall was taken into considered in the calculation as well. The power distributions of the main mode along the axial length are shown in Fig. 7, and the TE_{11} power distribution at the TE_{11} output port as a function of frequency is shown in Fig. 8. Figure 8 indicates that the conversion frequency from TE_{01} to TE_{11} is 99.646% at the frequency of 24.13 GHz. The longitudinal electric field distribution on the 2-D cut plane of the transition is shown in Fig. 9.

2.3 Simulation and design of TE_{11}-HE_{11} converter

The TE_{11} to HE_{11} mode conversion is based on a circumferentially corrugated waveguide where the depth of the corrugation is varied from $\lambda/2$ to $\lambda/4$ over a length L. The depth profile is defined in Eq. 10.

$$d(z) = \left(\frac{\lambda}{2}\right) - \left(\frac{\lambda}{4}\right)\left(\frac{z}{L}\right)^N \quad . \quad (10)$$

The depth profile for the corrugation defined in the equation above was optimized by searching for values of

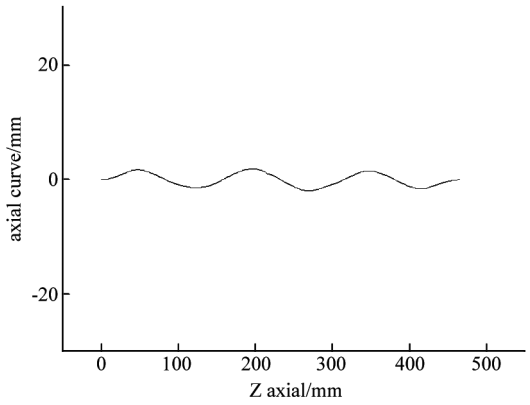

Fig. 6　Shape of the TE_{01} to TE_{11} mode converter showing the displacement of the axis versus length
图 6　轴向位移 TE_{01}-TE_{11} 模式转换器的形状

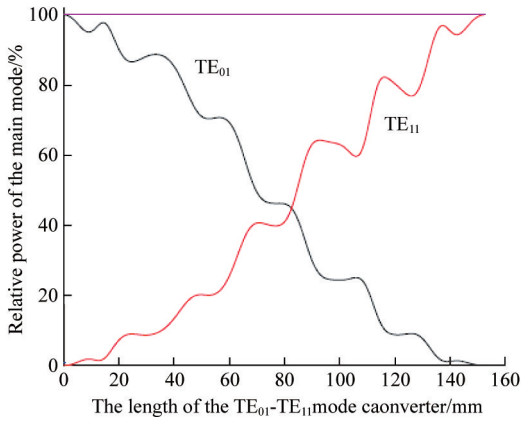

Fig. 7　Power distribution along the curvilinear path length Z
图 7　沿弯曲轴线路径 Z 的模式转换效率分布

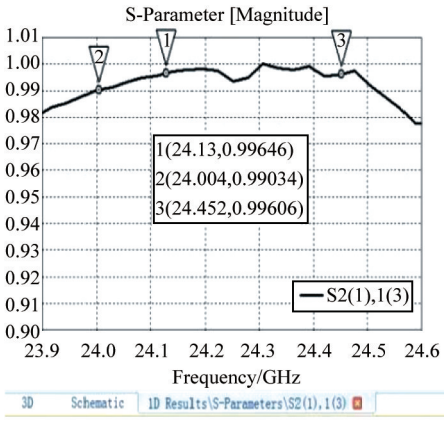

Fig. 8　Power distribution of the TE_{11} mode with the change of frequency at the output port
图 8　随着频率改变的 TE_{11} 模式输出端口的功率分布图

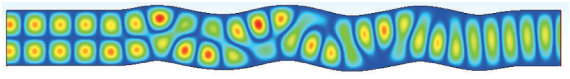

Fig. 9　Field distribution on the 2-D longitudinal cut plane of the TE_{01}-TE_{11} converter
图 9　二维切面的 TE_{01}-TE_{11} 转换器的场分布图

N and *L*. We used the structure above to realize the TE_{11}-HE_{11} mode conversion. The breakdown problem in corrugate gap can be solved by analyzing the chamfering to the converter. The 3-D model of the converter is shown in Fig. 10.

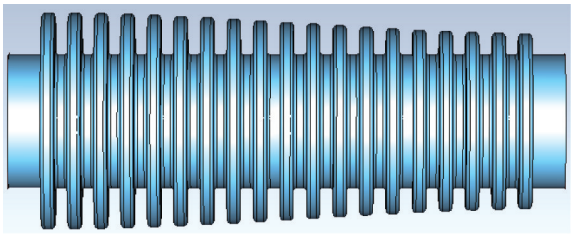

Fig. 10　CST model of the TE_{11}-HE_{11} mode converter
图 10　使用 CST 建模的 TE_{11}-HE_{11} 模式转换器

The calculation and the simulation by Microwave Studio CST software are shown in Fig. 11 and Fig. 12, respectively. At the frequency of 24.13 GHz, the TE_{11} power is 85.25% and the TM_{11} power is 14.28%, which satisfy the theoretical requirement on the power contents of the TE_{11} and TM_{11} in the HE_{11} mode, the HE_{11} power is 99.53%. Figure 14 shows the electric field distribution of the output port of the mode converter. Given the field distribution in the axial-cut plane of the converter showed in Fig. 14, the total efficiency of TE_{01}-HE_{11} converter can be calculated as the product of each part's conversion efficiency: 99.89% * 99.646% * 99.53% = 99.069%.

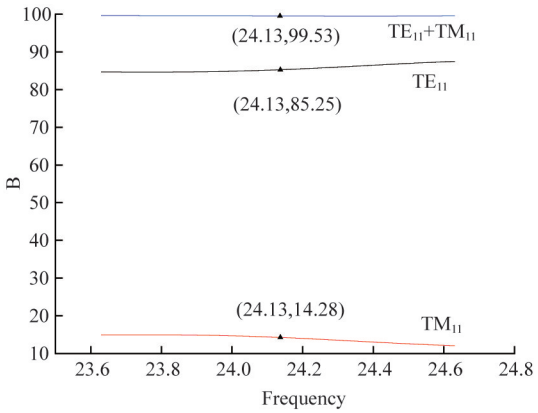

Fig. 11　calculated result by a coding program
图 11　通过编写代码计算出的结果

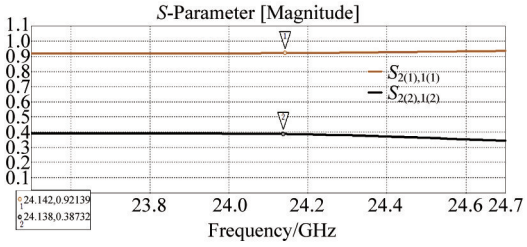

Fig. 12　TE_{11} and TM_{11} mode amplitudes in coding program output port by CST software
图 12　通过 CST 仿真得到的 TE_{11} 和 TM_{11} 模振幅

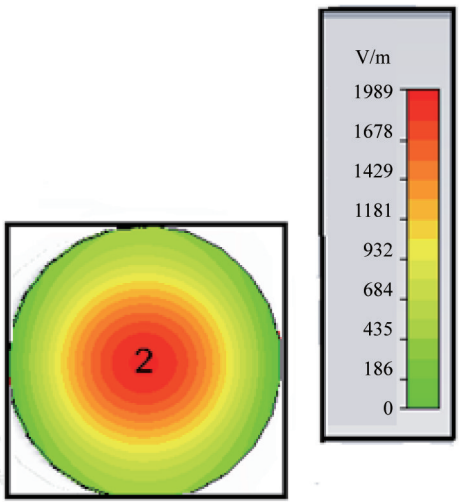

Fig. 13 Electric field distribution of the output port of the TE_{11}-HE_{11} mode converter
图 13 模式转换器输出端口的电场分布图

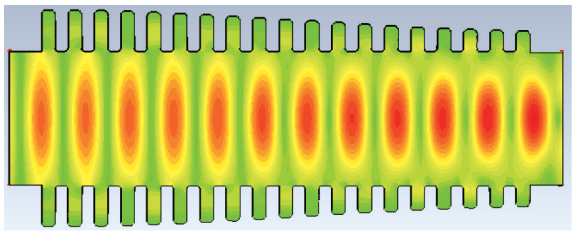

Fig. 14 The axial field distribution of TE_{11}-HE_{11} output port of the mode converter mode converter
图 14 TE_{11}-HE_{11} 模式转换器出书端口的轴向场分布图

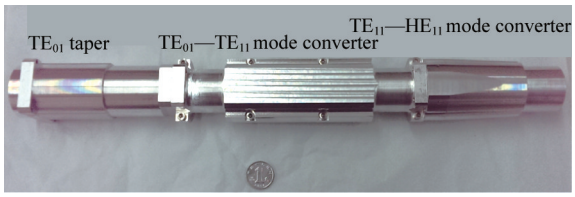

Fig. 15 The physical picture of the TE_{01}-HE_{11} system
图 15 TE_{01}-HE_{11} 系统的实物图

3 Test

A new assembly, as shown in Fig. 15, was built to apply the mode conversion system. The cold test was also practiced to the system. The far field distribution of output mode under the cold test is shown in Fig. 16. Similarly, we tested the TE_{11}-HE_{11} mode converter as well, and the far field distribution of output mode under the cold test is shown in Fig. 17. The cold tests indicate that the system we designed could perform functionally in mode conversion.

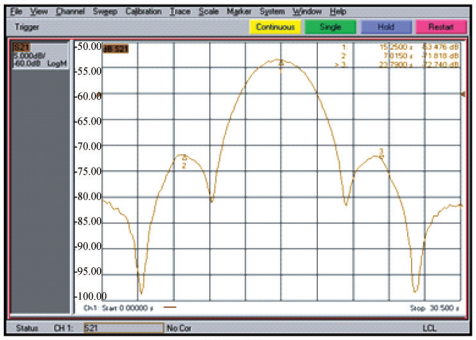

(a) E-Plane

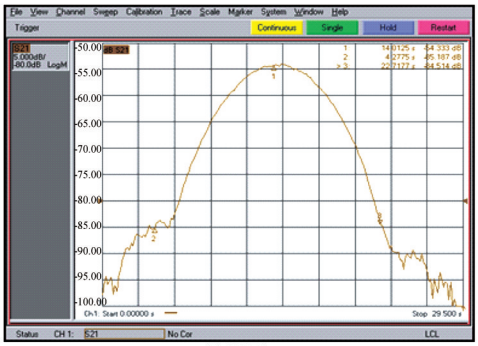

(b) H-Plane

Fig. 16 The radiation field distribution of the TE_{01}-TE_{11} mode converter
图 16 TE_{01}-TE_{11} 模式转换器的辐射场分布图

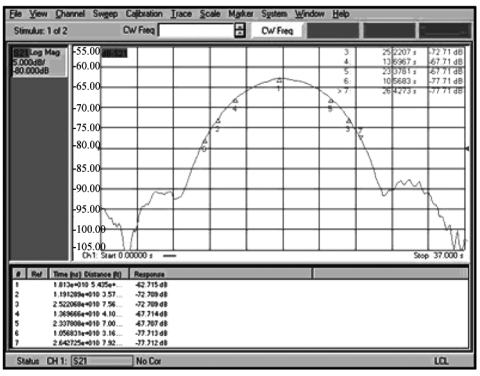

(a)E-plane

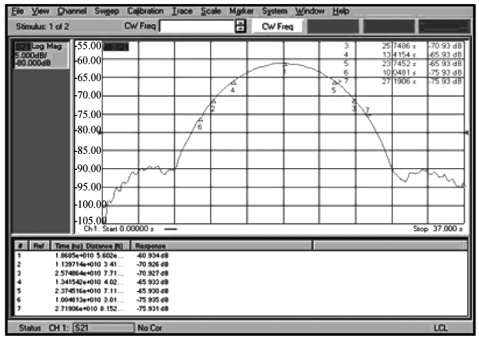

(b) H-plane

Fig. 17 The radiation field distribution of the TE_{11}-HE_{11} mode converter
图 17 TE_{11}-HE_{11} 模式转换器的辐射场分布图

4 Conclusion

Based on the coupled wave theory and the mode-matching method, a waveguide system to generate HE_{11} mode was designed and analyzed in this paper. The calculations and simulations showed that the system performed well in transforming from TE_{01} to HE_{11} mode. The cold tests to the waveguide system confirmed that the system we designed has great performance in mode conversion.

References

[1] Thumm M, Jacobs A, Sorolla Ayza M. Design of short high-power TE_{11}-HE_{11} mode converters in highly overmoded corrugated waveguides [J]. *IEEE Transactions on Microwave Theory & Techniques*, 1991, **39**(2):301 - 309.

[2] Denisov G G, Kulygin M L. Numerical Simulation of Waveguide TE_{01}-TE_{11} Mode Converter Using FDTD Method [J]. *Journal of Infrared, Millimeter, and Terahertz Waves*, 2005, **26**(3):341 - 361.

[3] Lyneis C, Benitez J, Hodgkinson A, *et al*. A mode converter to generate a Gaussian-like mode for injection into the VENUS electron cyclotron resonance ion source [J]. *Review of Scientific Instruments*, 2014, **85**(2):02A932 - 02A932.

[4] LI Hong-Fu, MANFRED THUMM. Mode conversion due to curvature in corrugated waveguides [J]. *International Journal of Electronics*, 1991, **71**(2):333 - 347.

[5] LI Hong-Fu, MANFRED THUMM. Mode coupling in corrugated waveguides with varying wall impedance and diameter change [J]. *International Journal of Electronics*, 1991, **71**(5):827 - 844.

[6] NIU Xin-Jian, ZHU Xian-Neng, LIU Ying-Hui, *et al*. Study of Ka-band TE_{01} to TE_{11} Mode Converters with Parallel Input and Output Waveguides [J]. *Journal of Infrared Millimeter and Terahertz Waves*, 2014, **35**(2):179 - 186.

[7] NIU Xin-Jian, LEI Chao-Jun, Liu Ying-Hui, *et al*. A Study on 94 GHz Low-Voltage, Low-Current Gyrotron [J]. *IEEE Transactions On Electron Devices*, 2013, **60**(11): 3907 - 3912.

[8] NIU Xin-Jian, LI Hong-Fu, XIE Zhong-Lian. Analysis of 8 mm high power TE_{01} TM_{11} mode converter in overmoded waveguide [C]. Bei-Jing: ICMMT 2002.

(上接 5 页)

[17] Xu C M, Xu X L, Xu J, *et al*. Composition dependence of the Raman A_1 mode and additional mode in tetragonal Cu-In-Se thin films [J]. *Semiconductor Science and Technology*, 2004, **19**: 1201.

[18] Han J, Liao C, Jiang T, *et al*. Investigation of copper indium gallium selenide material growth by selenization of metallic precursors [J]. *Journal of Crystal Growth*, 2013, **382**: 56.

[19] Turcu M., Pakma O, Rau U, Interdependence of absorber composition and recombination mechanism in $Cu(In,Ga)(Se,S)_2$ heterojunction solar cells [J]. *Applied Physics Letters*, 2002, **80**: 2598.

[20] Dieing T, Hollricher O, Toporski J, *Confocal Raman Microscopy* [M]. Berlin Heidelberg, Springer-Verlag, 2010: 73 - 74.

[21] Márquez R, Rincón C, Defect physics of the ordered defect compound $CuIn_3Se_5$ [J]. *Solar Energy Materials & Solar Cells*, 2002, **71**: 19.

[22] Dullweber T, Hanna G, Rau U, *et al*. A new approach to high-efficiency solar cells by band gap grading in $Cu(In,Ga)Se_2$ chalcopyrite semiconductors [J]. *Solar Energy Materials & Solar Cells*, 2001, **67**: 145.

[23] Liao K H, Su C Y, Ding Y T, Effects of Ga accumulation on the microstructure of $Cu(In_{1-x},Ga_x)Se_2$ thin films during selenization [J]. *Journal of Alloys and Compounds*, 2013, **581**: 250.